

A New Posthole Seismometer at Concordia Permanent Research Facility in the Heart of the Icy East Antarctic Plateau

Maxime Bès de Berc^{1,2} , Dimitri Zigone^{1,2} , Peter Danecek³ , Alain Steyer¹, Francesco Zanolin³ , Alessia Maggi^{1,2} , Jean-Yves Thoré², Armelle Bernard², Hervé Blumentritt², Sophie Lambotte^{1,2} , Jean-Jacques Lévêque^{1,2}, Luis Rivera^{1,2} , Olivier Alemany⁴, Philippe Possenti⁴, Martin Vallée⁵ , Eléonore Stutzmann⁵ , Adriano Cavaliere³ , Nathalie Cotte⁶, Stefano Marino³ , Baptiste Gombert^{1,2,7} , Wenceslas Marie-Sainte⁸, Nicolas Leroy⁵, Constanza Pardo⁵ , Frédérick Pesqueira⁵, and Céleste Broucke⁵ 

Abstract

In the Southern Hemisphere, the prevalence of oceans and the difficulty of access to land result in reduced coverage of seismological stations, limiting our detailed knowledge of Earth's structures and of large earthquakes sources. This situation is exacerbated inside the antarctic continent, where only two permanent seismic stations are currently available (IU.QSPA at South Pole and G.CCD). The CCD station, built in early 2000s with state-of-the-art surface instrumentation and located at the French–Italian Concordia base (75° S, 123° E), has been providing seismological data since 2008. However, it suffers from several problems: the vault is deformed by the hydrostatic pressure of the snow, the firn waveguide traps anthropogenic noise from the base causing strong noise below 1 s, and a coupling defect limits the performance above 30 s on the horizontal channels. To ensure the continuity of CCD and to improve its overall performance, we started in 2014 to plan the installation of a borehole seismometer at the site. In this article, we describe in detail this renovation of CCD and some examples of data analysis. The new borehole sensor shows that short-period disturbances are largely attenuated (–20 dB at 0.1 s) compared to the surface installation and that the horizontal channels have a lower noise level at long periods (–8 dB at 100 s). Data for all components are below the standard noise model between 0.1 and 0.2 s, which makes this sensor one of the quietest installations in the world for this bandwidth. For periods > 600 s we observe atmospheric pressure-related perturbations on the vertical component. Despite this problem, the new CCD borehole station is a success with better-than-expected performances at all periods < 600 s. The data produced are now distributed in the world's data centers as G.CCD.20 and we encourage the scientific community to use the data for all studies requiring seismograms from Antarctica.

Introduction

Since the late 70s, the continuous development of global broadband seismological networks has significantly increased the worldwide coverage of seismic stations. This effort has been providing key seismic records to improve our understanding of the solid Earth structure and of the source parameters of major earthquakes (see companion article Leroy *et al.*, submitted in the same special issue of *SRL*, and Ringler *et al.*, 2022 for extensive reviews of the science made possible by global seismic networks). However, despite improvements in recent years, the coverage of the Southern Hemisphere remains significantly lower than the Northern Hemisphere. This lack of seismic stations is even more striking in the southern high

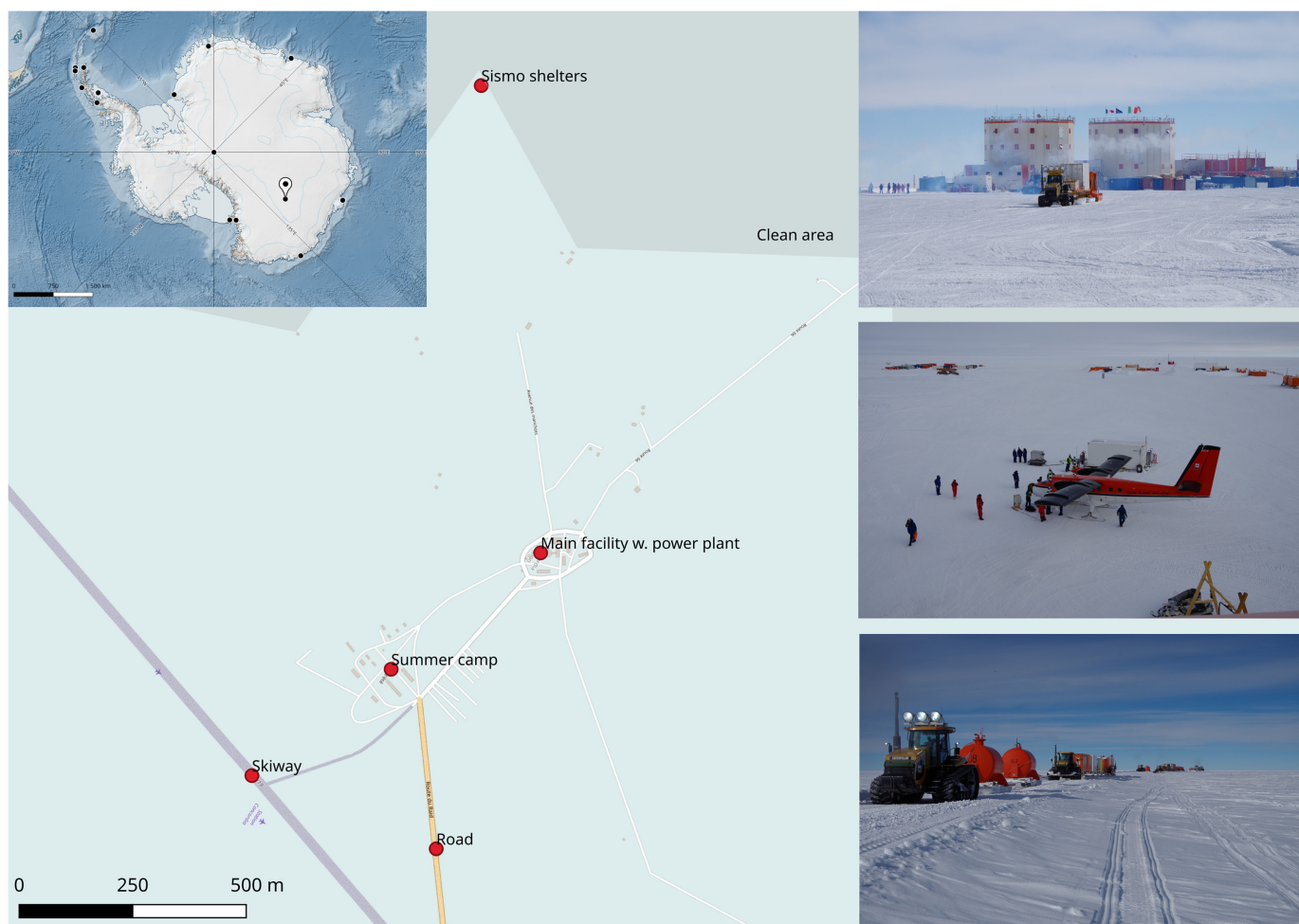
Cite this article as Bès de Berc, M., D. Zigone, P. Danecek, A. Steyer, F. Zanolin, A. Maggi, J.-Y. Thoré, A. Bernard, H. Blumentritt, S. Lambotte, *et al.* (2023). A New Posthole Seismometer at Concordia Permanent Research Facility in the Heart of the Icy East Antarctic Plateau, *Seismol. Res. Lett.* **XX**, 1–15, doi: [10.1785/0220230188](https://doi.org/10.1785/0220230188).

Supplemental Material

1. Université de Strasbourg/CNRS, Institut Terre et Environnement de Strasbourg, Strasbourg, France, <https://orcid.org/0000-0002-1824-966X> (MBdB); <https://orcid.org/0000-0003-2383-8271> (DZ); <https://orcid.org/0000-0001-8859-8948> (AM); <https://orcid.org/0000-0003-1078-3419> (SL); <https://orcid.org/0000-0002-0726-5445> (LR); <https://orcid.org/0000-0002-6373-4373> (BG); 2. Université de Strasbourg/CNRS, Ecole et Observatoire des Sciences de la Terre, Strasbourg, France; 3. Istituto Nazionale di Geofisica e Vulcanologia, Centro Nazionale Terremoti, Rome, Italy, <https://orcid.org/0000-0002-2522-4567> (PD); <https://orcid.org/0000-0002-8669-5266> (FZ); <https://orcid.org/0000-0003-2888-324X> (AC); <https://orcid.org/0000-0001-9379-269X> (SM); 4. Centre National de la Recherche Scientifique (CNRS), Institut de Géophysique de l'Environnement (IGE), Grenoble, France; 5. Université Paris Cité, Institut de physique du globe de Paris, CNRS, Paris, France, <https://orcid.org/0000-0001-8049-4634> (MV); <https://orcid.org/0000-0002-4348-7475> (ES); <https://orcid.org/0000-0003-1601-8718> (CP); <https://orcid.org/0009-0006-6959-1103> (CB); 6. Université Grenoble Alpes, Université Savoie Mont Blanc, CNRS, IRD, IFSTTAR, Institut des Sciences de la Terre, Grenoble, France; 7. Now at Collecte Localisation Satellite, Ramonville-St-Agne, France; 8. Institut Polaire Français Paul-Emile Victor, Plouzané, France

*Corresponding author: mbesdeberc@unistra.fr

© Seismological Society of America



latitudes due to complex logistical constraints associated with the prevalence of oceans above 50° S and the harsh environmental conditions in Antarctica. This results in only 15 permanent broadband stations in Antarctica, of which only two are located in the interior of the continent: South Pole (QSPA station, from Global Seismic Network, [Albuquerque Seismological Laboratory/U.S. Geological Survey \[USGS\], 2014; Anthony et al., 2021](#)) and Concordia (CCD station, from GEOSCOPE network, [Institut de physique du globe de Paris \[IPGP\] and École et Observatoire des Sciences de la Terre de Strasbourg \[EOST\], 1982](#)). Based on six decades of data from South Pole stations, [Anthony et al. \(2021\)](#) recently provided a review of all the science made possible with stations from inside the Antarctic continent and why it is critical that global seismic networks maintain continuous broadband seismic recordings from those undersampled regions.

In the early 90s, the French and Italian Polar Institutes asked for expressions of interest for a scientific base in the heart of the antarctic continent near dome C—1200 km from the French coastal base Dumont d’Urville and at 3250 m elevation—where glaciological drilling was performed in the 70s. J. Trampert at École et Observatoire des Sciences de la Terre de Strasbourg (EOST) and A. Morelli at Istituto

Figure 1. Location of the seismological station in the area of Concordia research facility. Upper left inset: location of Concordia (75° S, 123° E) in Antarctica, together with current permanent seismic stations (black dots). Right-side insets (from top to bottom): pictures of Concordia main base, Twin Otter planes and trucks convoy used to bring personnel and logistics (pictures by M. Bès de Berc, French Polar Institute, Centre National de la Recherche Scientifique [CNRS]). The color version of this figure is available only in the electronic edition.

Nazionale di Geofisica e Vulcanologia (INGV) wrote the first draft of a plan for an observatory seismic station at this location to complement the only existing point of recording from inside the antarctic continent at that time (IU.SPA at South Pole, replaced by IU.QSPA station in 2003, see [Anthony et al., 2021](#)). After the construction of the French–Italian scientific base Concordia (75° S, 123° E, see Fig. 1) was decided, the project for a seismic station was supervised by J.-J. Lévêque (EOST) and A. Morelli (INGV) and tests started in 1998. The seismological station was progressively constructed over six summer campaigns between 1999 and 2004, at the same time as the scientific base itself. Two seismometers have been

running continuously since the permanent occupation of Concordia in December 2004. In the first 3 yr of operation, the station served as a testbed to determine the best practices in running a seismological station on the east Antarctic plateau where the conditions are particularly extreme with temperatures ranging from -30°C during the austral summer to -80°C during the winter. The Concordia data were finally opened using the station code CCD in 2007, and their quality reached the required standard for wider distribution in 2009. Finally, CCD changed status from an experimental to a permanent observatory station and integrated the global GEOSCOPE network in 2010.

The original seismological station is installed at 1 km from the Concordia main facility and is composed of an artificial vault made of three shipping containers that were buried about 12 m in the snow to protect the instruments from the most extreme temperature conditions and noise sources. A 45 m tunnel below the upper snow layers connects the vault to a shelter where all the acquisition electronics (digitizers, computers, state of health systems, etc.) are installed. Figure 2d presents a sketch of the vault and tunnel. At the start of the station in 2004, the instrumentation was composed of two Streckeisen STS-2 seismometers installed in a niche cut in the wall of the vault. One STS-2 was heated at -30°C (location code 00), whereas the other was operating at room temperature -54°C (location code 10). The data were first acquired by a unique Quanterra Q4120 then completed with a Q330 digitizing the colder STS-2 and ensuring strict redundancy. This latter sensor was stopped in 2010 because of performances issues and a new Nanometrics Trillium 240 was installed on a granite plate fixed in the snow at the bottom of the vault. Because the performances of the T240 were better than those of the STS-2, the T240 was assigned the location code 00, whereas the heated STS-2 was assigned location code 10. In addition, the Q4120 and the Q330 were replaced by two Quanterra Q330S and associated with industrial computers running the SeisComp (Helmholtz-Centre Potsdam—GeoForschungsZentrums [GFZ] German Research Centre for Geosciences and gempa GmbH, 2008) toolkit for data backup and real-time stream. In 2011, the data from CCD station were made available in real-time through the very-small-aperture terminal (VSAT) internet connections provided by the French and Italian polar institutes. The vault design was state-of-the-art twenty years ago and provided a good environment with a constant temperature of -54°C all year round to successfully run a broadband seismological station. However, several issues related to both safety and seismological performances have emerged through time:

1. Because of its short distance to the base, the station suffers from increased diurnal noise (up to 40 dB) at periods below 0.25 s (Fig. 2c), especially in the summer season. Anthropogenic noise is trapped in a firn layer, which forms

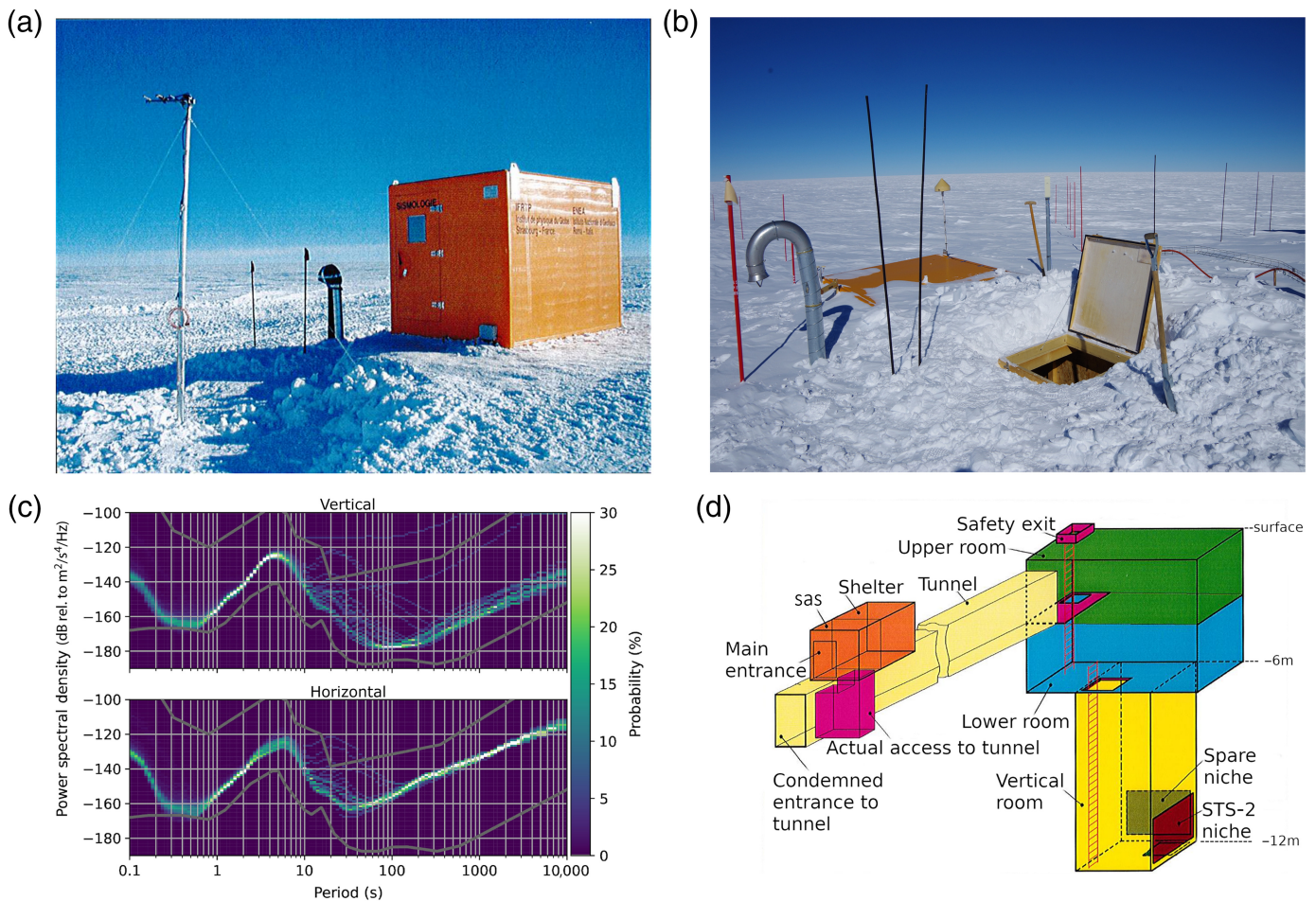
a 90–100-m-thick waveguide (Albert, 1998; Diez *et al.*, 2013), and is picked up easily by both seismometers.

2. Another limitation comes from the hydrostatic pressure of the snow, which is continuously deforming the metallic structures of the containers: we have recorded many container cracking events on the seismograms, and we have seen visual evidence of structural deformations inside the tunnel and the vault. Those deformations have rendered the floor uneven and slippery, posing safety problems for the personnel maintaining the station. The bottom of the vault is only reachable by descending two 6-m-high metal ladders which makes any emergency recovery difficult should an accident occur in the vault.
3. The accumulation of snow above the shelter and the emergency exit in the vault have made the entrances accessible only via regularly raised hatches (Fig. 2b). The accumulation of snow also increases the load on the tunnel between the shelter and the cave. The roof of this tunnel, made of plywood, already shows deformations and might eventually collapse from this increasing load.
4. Finally, the hydrostatic pressure of snow and ice limit the scientific use of the data. Seismometers placed in the primary niche cut in the wall of the vault (STS-2) are subject to regular increase of tilt, and consequently have to be recentered remotely every 6–7 weeks and releveled manually every year (Fig. S1, available in the supplemental material to this article). The main seismometer (T240) installed at the bottom of the vault is less affected, requiring only two recenterings per year, but still suffers from a coupling defect that limits its performance at long periods (>30 s) on the horizontal channels (Fig. 2c). The recentering operations severely disrupt the seismic signal, making the data unusable for applications requiring long time spans of unperturbed data (e.g., normal-mode studies) for which stations at high latitudes present a strong interest (e.g., Anthony *et al.*, 2021).

Preparation and Realization of the New Borehole Station

Infrastructure design

In 2014, we started discussions with all involved partners and decided to install a borehole seismometer to provide a more stable configuration than the current vault. This concept is similar to the design of seismic station QSPA, the current observatory installed 8 km from the American Amundsen–Scott base at the South Pole (Anderson, 2003; Anthony *et al.*, 2021). A borehole station has the advantage of greatly reducing the noise from thermal effects, tilting, and anthropogenic activity, in particular if the borehole reaches a depth below the firn waveguide (Albert, 1998). The antarctic polar ice sheet has a steep near-surface seismic velocity gradient caused by firn densification in the top 200 m. This steep gradient forms a



waveguide that traps seismic energies by refracting downgoing seismic waves back to the surface. [Albert \(1998\)](#) demonstrated the key role played by this waveguide by computing noise propagation in the firn layer at South Pole. He showed that the transmission loss for vertical particle velocity is very low at short periods (<0.1 s) for waves moving out from the surface noise source. By contrast, significant improvement is achieved by placing the sensor beneath the firn layer; here, transmission loss reaches up to 100 dB at 0.1 s at a distance of 10 km. Those theoretical calculations have been verified with a noise survey of the South Pole site ([Anderson, 2003](#)), which validated the recommendation of [Albert \(1998\)](#) to place the sensor at 10 km from the base and at least at 200 m depth. Today's QSPA seismic station was installed successfully in 2003 at a site located 8 km away from the Amundsen Scott base and at a depth of 275 m, and achieved significant performance improvements for periods below 0.2 s compared to the former surface installation ([Anthony et al., 2021](#)).

Because of the issues associated with the historical infrastructure in Concordia, we designed the borehole to avoid anthropogenic noise coming from the main facility (periods below 1 s) while maintaining or even improving long-period performances. Because we aimed to deliver a new-generation observatory-grade station, needing a stable power supply and

Figure 2. Surface shelter installed (a) in 2002 and (b) its state in 2020. (c) The Trillium 240 (G.CCD.00) sensor inside the vault provide data described by probabilistic density functions (PDFs) for the whole year 2022. (d) The vault is built with buried containers in snow, accessible through a 45-m-long tunnel. The color version of this figure is available only in the electronic edition.

network connection, and had to respect predesignated clean areas dedicated to snow composition analysis in the vicinity, we were constrained to stay very close to the current site. Therefore, the borehole location has been chosen at 40 m from the existing shelter. Given the QSPA results, we decided to install the new sensor below the firn waveguide. At dome C, density measurements with depth have been performed in several boreholes including the European Project for Ice Coring in Antarctica (EPICA, see [Augustin et al., 2004](#)) deep borehole. The data show a steep increase in firn density from 0.3 g/m^3 at the surface to 0.85 g/m^3 at 100 m depth ([Bréant et al., 2017](#)). This is steeper than in the South Pole where a density of 0.85 g/m^3 is reached at 150 m depth. The firn density data constrain firn densification models that allow us to compute the depth at which the pores in the firn seal off

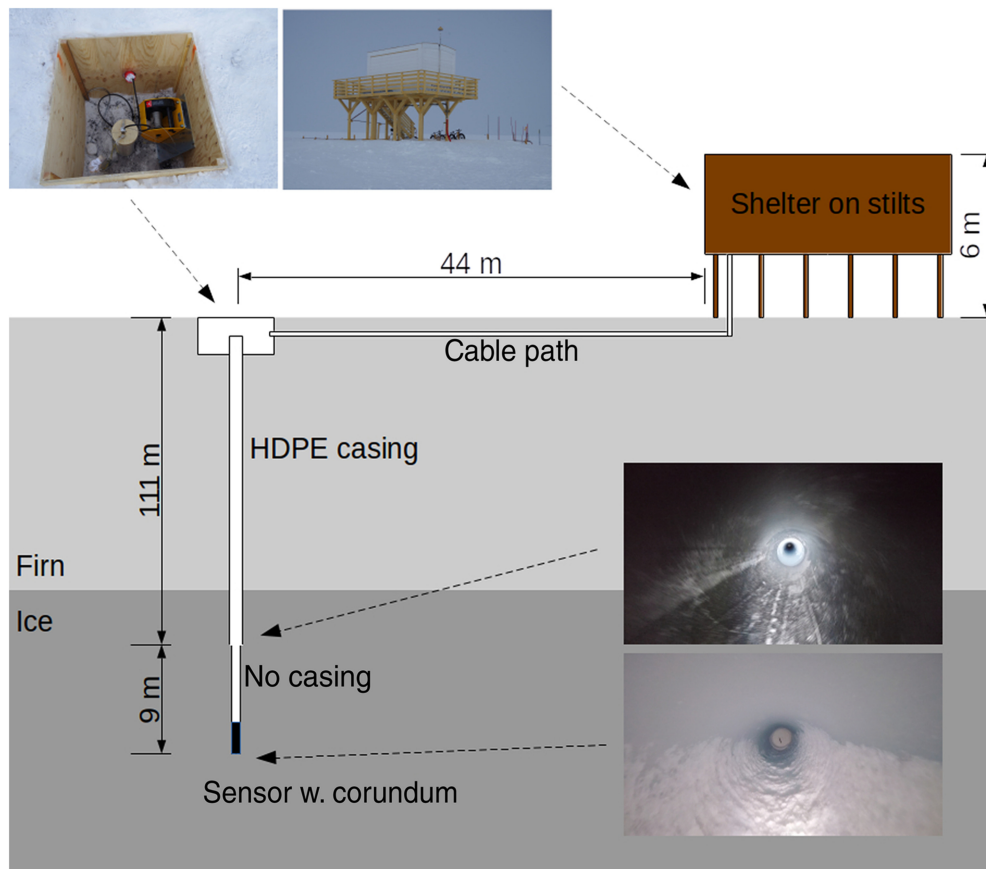


Figure 3. Newly built infrastructure including a 120 m deep borehole with HDPE casing and 6-m-high shelter on stilts. Firn to ice transition is estimated at 90–95 m. Figure is not to scale. The color version of this figure is available only in the electronic edition.

(lock-in-depth), which defines the waveguide thickness because the density gradient below remains close to 0. At dome C, the lock-in depth is estimated at 90–95 m (Bréant *et al.*, 2017), so we drilled the borehole to a depth of 120 m. The temperature at this depth is stable at -55°C . To keep the hole open in the long term, we installed casing tubes down to 111 m and left uncased the deeper part, which is in solid ice. Figure 3 presents a schematic of the borehole design. We built a 6-m-high new shelter on stilts, around 45 m away from the borehole (Fig. 3). It is not common in seismology to choose such a structure, which could pollute data with wind-induced vibrations. Despite the risk, because longevity was a strong requirement in design, this solution was chosen because it avoids snow accumulation and, therefore, allows the shelter to be used for longer. To limit wind pollution, the head of borehole and cable path were buried beneath the snow level.

Borehole drilling

The detailed specifications and the drilling operations of the borehole were planned and supervised by glaciologists

from the F2G (Plateforme Française de Forage Glaciaire) hosted at IGE (Institut des Géosciences de l'Environnement) in Grenoble (France).

We drilled the borehole in December 2018. A first hole with diameter 140 mm was drilled with a polar shallow drilling system composed of the drill itself (core barrel, outer tube, motor section, and antitorque section) with its winch, cable, and tower (see Fig. S6b). The drill was suspended in the borehole by an electric cable fixed to a suspension at the top of the drill. Below this suspension were the motor compartment and the antitorque section, which prevented rotation of the drill itself when the drill head rotated. The drill was driven from the surface by an operator through a control panel. We used a drilling speed of about 4 mm per second and produced ice cores in 1–2 m sections, depending on the depth. More than 50 runs were

required to reach the targeted depth of 120 m. After reaching this depth, the hole was widened to 220 mm to accommodate the casing tubes, which had an external diameter of 180 mm. To increase the borehole diameter (a process called reaming), we replaced the drill head and the lower part of the drill with a special cutting device connected directly under the motor section (Fig. S6c). The ice chips produced while reaming fell to the bottom of the borehole; we reused the normal drill to collect them. We proceeded in two steps, first reaming to a diameter of 180 mm, then to the target diameter of 220 mm.

For the casing, we used 6-m-long SDR13.6 PN12.5 white high-density polyethylene (HDPE) tubes from Pipestar Australia. We prepared the tubes by deicing them, removing the extremities that were not of the nominal diameter, chamfering the ends to avoid creating a bump with the welding machine, and so forth (Fig. S6e). The first tube was mounted on a stainless steel ring with cables attached to be able to pull out the casing from the surface in case of technical issues. The remaining tubes were then inserted one by one in the borehole and welded together with a Roweld P 160 Saniline welding machine from Rotenberger (Fig. S6a,c).

Instrumentation installation, configuration, and calibration

We chose to use a Nanometrics Trillium 120PH, third generation (T120-PH3-XC) posthole seismometer because

1. it is one of the few posthole 120 s sensors for which self-noise is low enough to permit long-periods analyses (-185 dB[acc.] at 100 s);
2. it is the only known model that has a polar version, allowing it to operate at temperatures down to -50°C ; and
3. it had a small enough diameter (143 mm) to allow us to drill the borehole with the tools available in Concordia.

Before installing the sensor, we dropped about 15 kg of corundum sand into the borehole and flattened it with a 10 kg cylindrical weight. We then attached a 2 mm diameter stainless steel cable on the seismometer's eyebolt and clamped the sensor cable and the stainless steel cables together 1 m above the eyebolt and then every 20 m. We lowered the instrument with a tripod-mounted low-gear winch, which allows one to adjust the sensor cable's slow descent with very fine vertical adjustment, particularly necessary when the seismometer was at the bottom of the borehole (Fig. S6f). After reaching the bottom, we kept the instrument upright by maintaining tension on the stainless steel cable and dropped about 5 kg more of corundum sand, to keep the seismometer vertical, then released the tension on the cable. All operations at the bottom were monitored by a digital bubble available on the sensor and accessible via a web interface; the vertical tilt at the end of the installation was about 1° . We then dropped about 35 kg more corundum sand and centered the sensor. Finally, we closed the borehole at the surface using two foam and wood half cylinders on top of the casing. The last clamp between the cables lies on this custom cork, which is permeable to air. Because the cable length from the seismometer to the shelter is about 200 m long, we power the sensor with an external 24 V battery pack. We digitize the seismic signals using a Quanterra Q330S. Both digitizer and batteries are installed inside the wooden shelter on stilts, in a box at a controlled temperature of 8°C (Fig. 3).

After a settling period of 2 days, we started preliminary analysis of data. Although we expected a strong improvement on all periods below 1 s compared with surface sensor, this improvement was limited because we reached the digitizer self-noise. To improve our sensitivity to low-amplitude seismic signals in this period range, we activated the digitizer $\times 30$ preamplifier that lowers the self-noise (Fig. 4).

As a final part of installation process, we calibrated the three components of the T120PH by injecting into its calibration coils a 156 mV amplitude step signal, generated by the digitizer. This is equivalent to an acceleration step of 1.56 mm/s². For better accuracy, we calculated the periods and damping of the seismometer components by fitting their response curves to the falling edges of the acceleration steps.

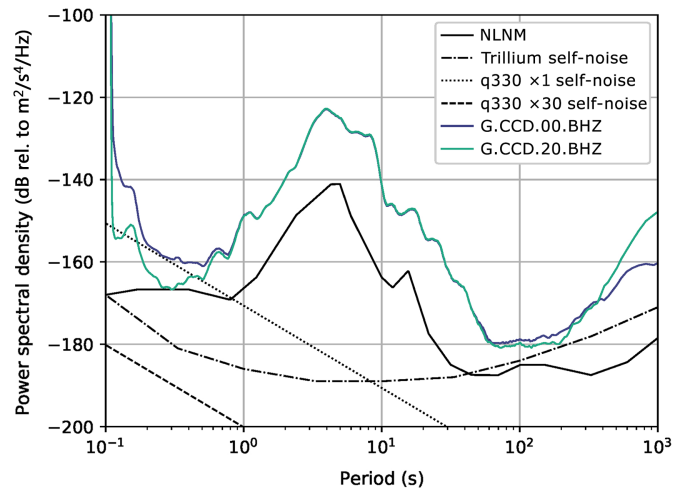


Figure 4. Typical power spectral densities (PSDs) of surface (G.CCD.00.BHZ, without preamplifier activation) and borehole (G.CCD.20.BHZ, with preamplifier activation) vertical sensors, compared with digitizers (preamplifier $\times 1$ dotted line, pre-amplifier $\times 30$ dashed line) and sensor self-noises. The period of time is 21 July 2020 from 00:00 to 12:00 UTC. Vault sensors preamplifiers have been later activated on 24 December 2021 (G.CCD.00) and 22 December 2021 (G.CCD.10). The color version of this figure is available only in the electronic edition.

We had performed calibration with the same method before shipping the instrument to Antarctica, so we could compare its performance at laboratory (20°C) and in situ (-55°C) operating temperatures (Table 1). The polar conditions do not seem to affect the damping but do increase the natural period of the individual sensors by about 1 s, slightly more than the 0.5% uncertainty on period and damping provided by the manufacturer. Data are available since 11 January 2020 under location code 20.

Noise Performances and Interfering Signals

To evaluate the reduction in Earth's ambient noise due to the installation of a borehole sensor, we computed probabilistic density functions (PDFs; Fig. 5a, McNamara, 2004) over long time windows (1 yr) and the ratio of power spectral densities (PSDs) between borehole and vault sensors over shorter time windows (3 days; see Fig. S2). Very-long-period noise (>200 s) is remarkably low and stable on the horizontal components, which show no evidence of tilt; it is below the vertical noise for periods above 2000 s. The Earth's noise level recorded at Concordia might lie below the new low-noise model (Peterson, 1993) at around 0.3 s during the quietest times (down to -171 dB on vertical component and -174 dB in horizontal components, Fig. 5b). These measurements demonstrate the permanent noise level improvement compared to the surface installation, up to 18 dB for vertical component and 25 dB

TABLE 1

Periods and Dampings of Borehole Trillium 120 PH Sensor Calibrated in Laboratory and In Situ, Compared with Theory

Parameter	Component	Theory	Lab	In Situ
Periods (s)	U	120.608	121.336	122.282
	V		121.330	122.315
	W		121.305	122.337
Dampings	U	0.703	0.706	0.7057
	V		0.7067	0.7065
	W		0.7062	0.7059

on horizontal components at all periods below 0.8 s (Fig. 5a). These values are time dependent, but remain between 8 and 25 dB at all times. The long-period improvement is clearly visible on most periods above 30 s, especially on horizontal components (up to 8 dB at 100 s); on the vertical component above 600 s; however, the borehole sensor becomes noisier than the surface one. To better highlight the noise reduction, we compare in Figure 5b the 10th percentile of the PDF for both the borehole and surface instruments along with those of the best borehole QSPA sensor (IU.QSPA.10). The short-period noise at Concordia remains higher than for QSPA station, due to its greater proximity to the main facility. Periods between 60 and 200 s are comparable on the vertical component between the borehole and surface with -180 dB at 100 s. On the horizontal components, the level is comparable to QSPA with a few dB improvements at periods of 100 s, confirming that the data recorded with this type of installation is less subject to ground tilt.

At higher frequencies, a linear spectrogram analysis for a typical week during the winter shows a predominant anthropogenic noise, between 5 and 10 Hz (0.1–0.2 s of period, Fig. 6). Lots of microevents, covering a large frequency range (2–10 Hz or 0.1–0.5 s), occur when winter-over staff use the track loader to fill the melter with snow to provide water. A permanent monochromatic signal at 4.5 Hz (0.222 s), visible all year long, is attributed to the main power plant. A wind-induced two-tone signal (3 and 3.2 Hz or 0.333 and 0.3125 s in periods) is also visible on all components and is attributed to the resonance of the shelter on stilts, 120 m above and 45 m away from the sensor.

At periods longer than 600 s, the performance of the vertical component decreases, as shown by the increased noise level at long periods in Figure 5b. To investigate this behavior at periods between 100 and 20,000 s, we computed the coherence between each of the three accelerometric components and the atmospheric pressure recorded by a microbarometer located close to the seismological shelter. Indeed, the atmospheric

pressure variations are known to be a candidate for causing such disturbances in acceleration, strong enough to become significant in velocity (e.g., [Beauduin et al., 1996](#)). The results of the coherence computations presented in Figure 7a show strong coherence between the borehole data and atmospheric pressure measurements. On the vertical component, coherence reaches 1 for periods longer than 1000 s. In this case, several physical mechanisms can be advocated to explain the pressure-generated signal. The most important contribution comes from buoyancy forces ([Ewing and Press, 1953](#)): pressure-induced variations in air density cause changes in the buoyancy force around the sensor mass and, thus, appear as long-period noise in the seismometer output signal. Fortunately, this effect can be dramatically reduced by housing the seismometer mechanism in a pressure-tight casing ([Wielandt and Streckeisen, 1982](#)). This is nowadays a standard practice. Two other contributions are due to the direct gravitational attraction between the atmospheric masses and the seismometer mass, and the elastic response of the solid Earth. Although these latter effects are unavoidable, it is now well established that at very long periods the residual signal in acceleration (e.g., removing the solid Earth tide contribution) is largely proportional to the atmospheric pressure variations (e.g., [Zürn and Widmer, 1995](#)). This observation allows the performance of an empirical data correction for these pressure-induced effects with a simple scaling factor (admittance) of around -3.5 nm/s²/hPa. This correction is nowadays routinely applied in normal mode analyses and tidal studies (e.g., [Crossley et al., 1995](#); [Zürn and Widmer, 1995](#); [Beauduin et al., 1996](#)). However, at CCD the admittance is much higher (Fig. 7b, green curve), reaching about 1600 nm/s²/hPa at periods longer than 12 hr. This high value is very close to the buoyancy factor computed by [Zürn and Wielandt \(2007\)](#) (1500 nm/s²/hPa). The magnitude of this pressure-related perturbation likely suggests an instrumental issue with the pressure tightness of the seismometer.

Examples of Scientific Applications

In this section, we show examples of scientific use of the new borehole sensor at CCD. Our goal is not to perform a complete scientific review but rather to give a few examples of what can be achieved with the improved data provided by the new CCD borehole instrument.

Firn resonance

Figure 5 shows that the new borehole sensor has noise levels below the NLMN between 1.5 and 5 Hz (0.2–0.6 s). Such performance was already observed at QSPA borehole sensors and make those two Antarctica stations among the quietest sites worldwide for those frequencies ([Ringler et al., 2020](#); [Anthony et al., 2021](#)). To further highlight the gain provided by a borehole sensor we followed the strategy of [Lévêque et al. \(2010\)](#) to evaluate the reduction of firn resonance using the

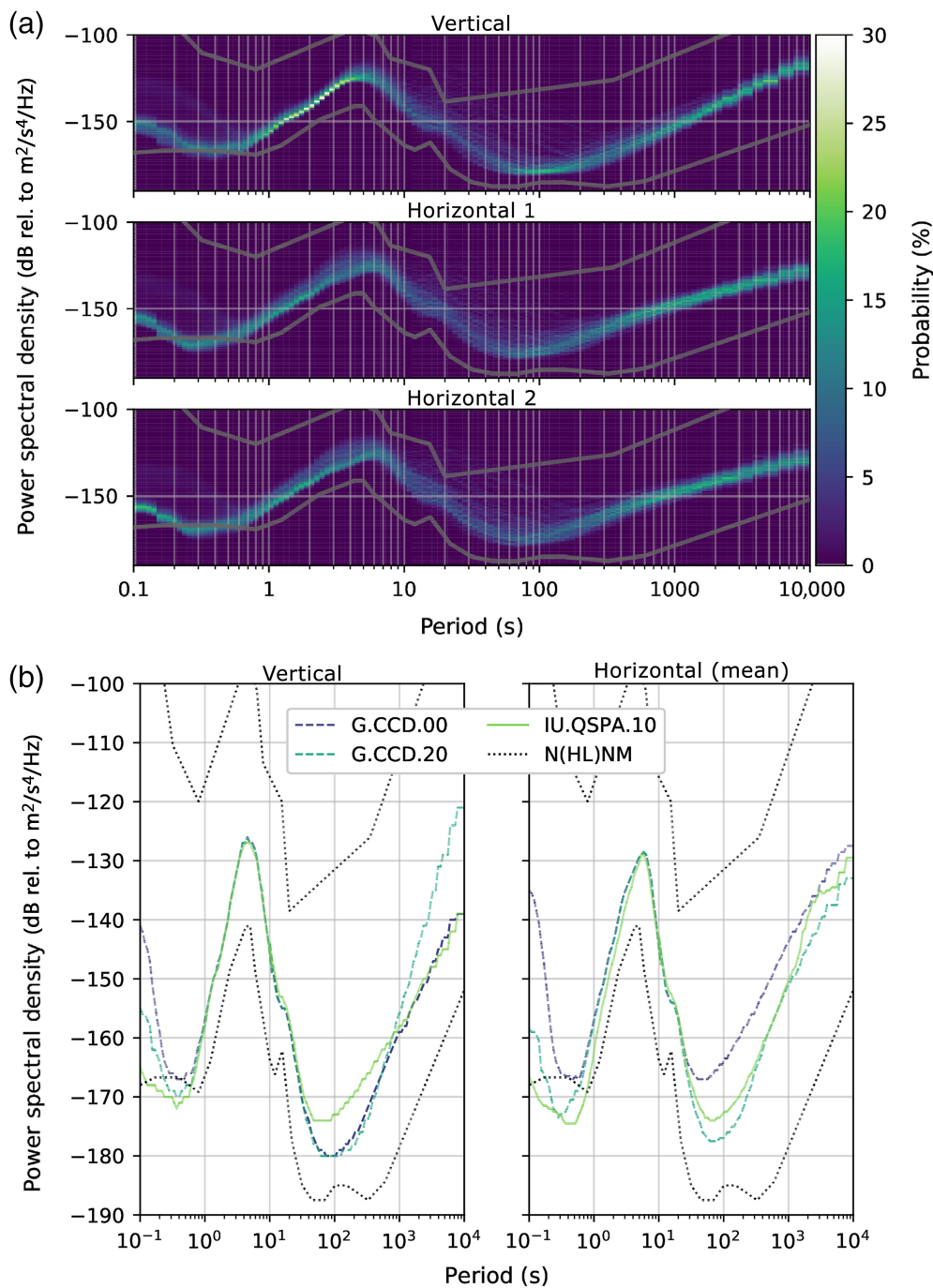


Figure 5. (a) All components PDFs computed on whole 2022 yr on borehole sensor data (G.CCD.20). 20 samples/s data are computed on 1 hr window length and contribute to periods between 0.1 and 10 s, whereas 1 sample/s data are computed on 1 day window length for periods between 10 and 10,000 s. (b) 10th percentile of PDFs of Concordia surface (G.CCD.00) and borehole (G.CCD.20) sensors, and QSPA (South Pole) borehole sensor, for both vertical and averaged horizontal components, computed on the same period. The color version of this figure is available only in the electronic edition.

provide stable and permanent anthropogenic noises. H/V spectral ratios are quite variable, ranging from around 1 for stations installed on rock to up to 10 in sedimentary basins, with a high-frequency peak that depends on the shear-wave velocity and the thickness of the uppermost layer (e.g., Lermo and Chávez-García, 1993; Gitterman *et al.*, 1996; Seekins *et al.*, 1996; Souriau *et al.*, 2007). At CCD, H/V spectral ratios for the STS-2 sensor (see the Introduction section for the history of sensors) show a clear high-frequency peak around 7 Hz, interpreted by Lévêque *et al.* (2010) as resulting from resonance in the firn caused by its low-shear-wave velocity, an interpretation confirmed by the peak's absence at the QSPA borehole station. Therefore, we expect to find the peak at around 7 Hz on the surface sensor and to lose it on the posthole sensor data. This reduction of the 7 Hz peak amplitude at 120 m depth is actually well observed in Figure 8.

The H/V results, presented in Figure 8, also indicate that both sensors show similar H/V spectra for frequencies below 1.5 Hz, with marked peaks at 0.4, 0.75, and 1.3 Hz similar to those observed by Lévêque *et al.* (2010). Above 1.5 Hz, the borehole sensor starts to show reduced amplitudes compared to the surface sensor, which seems to confirm that the borehole setup attenuates firn resonance effects.

horizontal-to-vertical (H/V) spectral ratio method on noise records (Nakamura, 1989; Field and Jacob, 1995; Bard, 1998). This method is widely used to compute the soil response to a seismic excitation, particularly in urban environments that

Earthquakes studies

Seismological stations in Antarctica are highly valuable for earthquakes studies because they fill a large azimuthal gap, particularly critical for earthquakes that occur in the southern

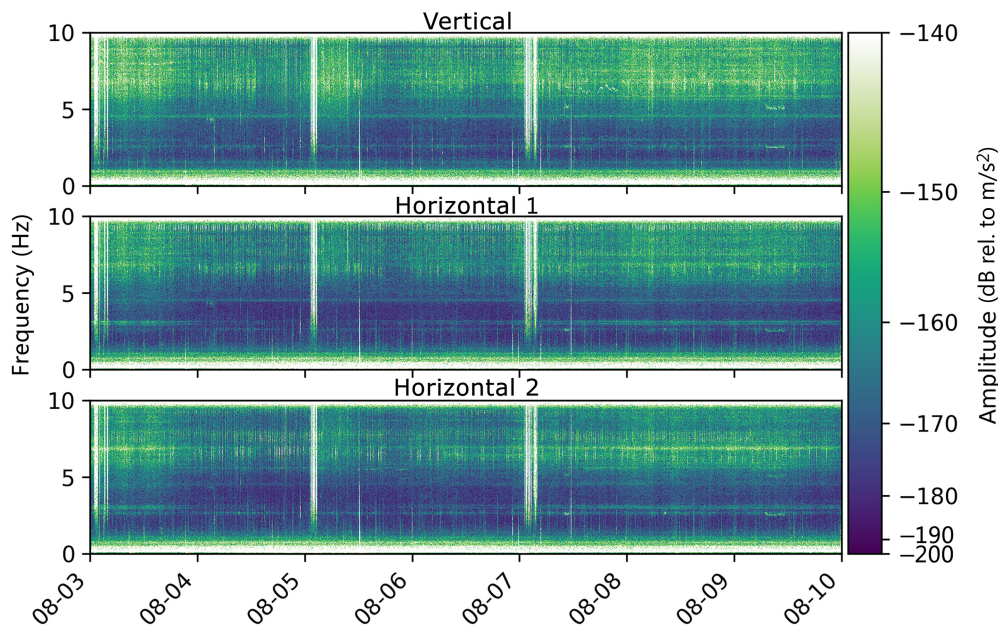


Figure 6. All components linear spectrogram on one week from 3 August 2021 to 10 August 2021, computed on 1 min window length, on borehole sensor. The color version of this figure is available only in the electronic edition.

hemisphere. As an illustration, CCD and other Antarctica stations were essential to understand the complex source of the 16 November 2016 M_w 7.8 Kaikoura earthquake in New Zealand (Duputel and Rivera, 2017). Thanks to their low-noise levels around 1 Hz (1 s), the inclusion of Antarctica stations also helps to improve the detection thresholds and local (M_L) and body-wave (m_B) magnitude estimates for smaller southern hemisphere earthquakes. Therefore, the unique locations of those stations play an important role in exhaustive monitoring and analyzes of Earth's seismicity (Ekström *et al.*, 2012; Benz, 2017).

Since 2014, GEOSCOPE observatory systematically characterizes large earthquakes (magnitude above 5.5–6) using a near-real-time implementation of the SCARDEC method (Vallée *et al.*, 2011). Focal mechanism, depth, moment magnitude, and source time function are routinely determined about 45 min after earthquake origin time and broadcast on the GEOSCOPE website, mailing lists, and Twitter. As a side product, synthetics computed for each sensor of the GEOSCOPE network allow continuous validation of the data and their metadata and estimates of the data quality. Figure 9 shows an example of earthquake characterization for a moderate magnitude event (7 June 2022 M_w 5.6 Sulawesi earthquake) and compares the CCD surface sensor (G.CCD.00) with the new borehole sensor (G.CCD.20). Data and synthetics show a close match for the new CCD borehole sensor, especially on the horizontal components where the improvement compared to the surface sensor is clearly visible. This example

illustrates the interest of incorporating the new sensor G.CCD.20 in systematic analyses of earthquakes properties.

Earth normal modes analysis

As presented in Figures 5 and 7, the new CCD borehole sensor presents strong atmospheric perturbations on the vertical component at long periods. These perturbations will affect normal modes analyses done with this new sensor. Considering one of the largest events recorded since the installation of the borehole sensor—29 June 2021 Alaska peninsula (M_w 8.2)—we compare the ability of the new sensor at CCD and the CGM3-T at QSPA to resolve Earth's low-frequency free oscillations (Fig. 10). On the

vertical components, neither sensor is able to resolve the normal modes below 1 mHz, and the noise level increases significantly below 1–1.5 mHz on the CCD sensor due to the stronger than expected atmospheric pressure effect (see paragraph about noise performances and interfering signals). Thus, at frequencies below 1.5 mHz (periods longer than approximately 600 s), the CCD borehole sensor performs slightly worse than the CGM3-T at QSPA or the CCD surface sensor (see Fig. S4). However, the quality of its horizontal components is comparable to that of the CGM3-T at QSPA at frequencies above 1 mHz and has slightly less noise below 1 mHz. The new borehole sensor has significantly better horizontal components compared to those of the surface sensor (see Fig. S4), which is unable to resolve any of the normal modes in the frequency band presented in Figure 10 (0.25–3 mHz). Such high-quality long-period data will improve the constraints that normal modes can bring on 3D heterogeneities in the isotropic and anisotropic velocity structure and the density structure of the Earth's interior; they will also help to determine the magnitude and focal mechanism of large events. Reducing the noise of the horizontal components, which we have achieved by improving installation at depth and sensor characteristics (e.g., Ringler *et al.*, 2020,2022) and reducing atmospheric noise (e.g., Zürn *et al.*, 2022), will improve their exploitation in analyses requiring toroidal modes. As an example, debate still continues on the presence of large-scale anisotropy in the deep mantle (e.g., Moulik and Ekström, 2014; Romanowicz and Wenk, 2017); additional robust measurements of toroidal

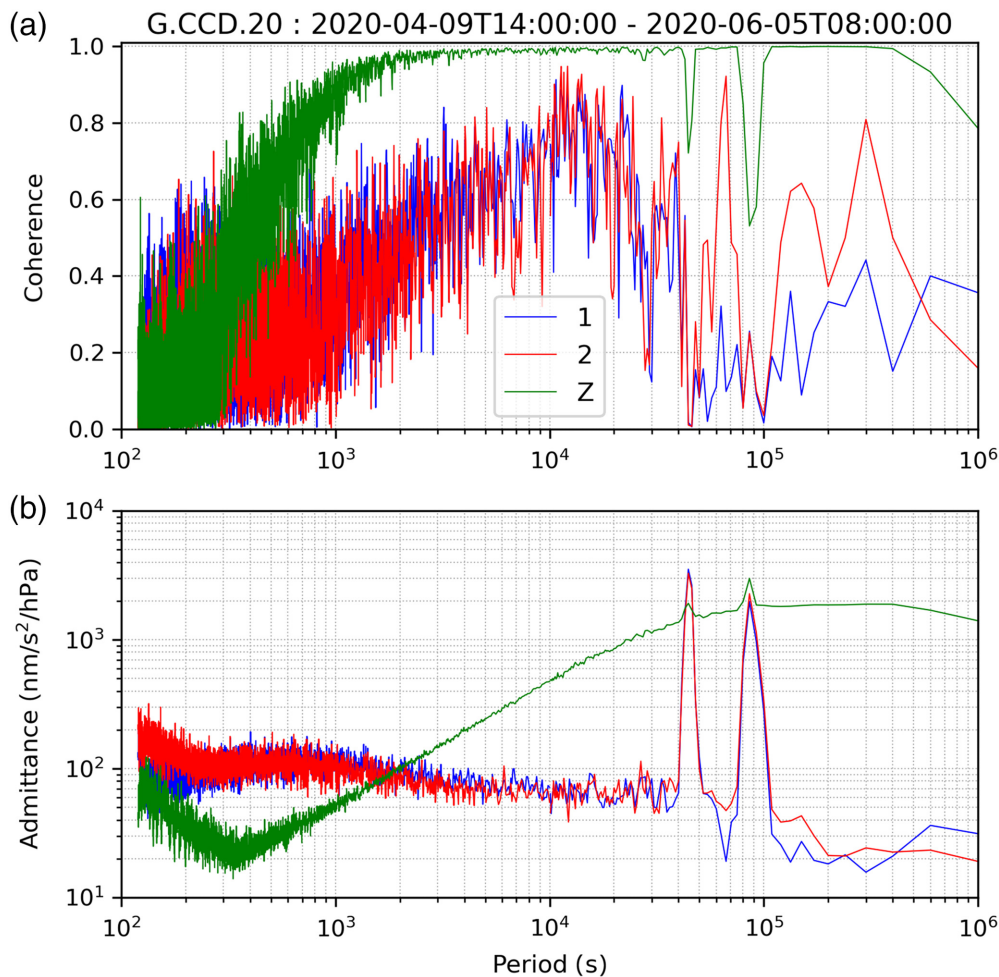


Figure 7. (a) Amplitude coherence between the three components in acceleration of the borehole seismometer at CCD and the atmospheric pressure (period of time analyzed: 9 April 2020–5 June 2020). Coherence is very good for the vertical component for periods larger than 600 s. (b) Admittance between each component (in acceleration) and the pressure. The two picks observed in the admittance curves correspond to the diurnal and semidiurnal Earth tides because they have not been removed from the data. The color version of this figure is available only in the electronic edition.

modes, which are few in number but recently extended (e.g., [Tromp and Zanzerkia, 1995](#); [Schneider and Deuss, 2021](#)), could contain critical clues for answering this question (e.g., [Restelli et al., 2023](#)).

Summary

We have presented the motivations, design constraints, infrastructure, installation, and performance of the Trillium 120 posthole seismometer that we installed at a depth of 120 m at the CCD seismological station near the Concordia research facility (Antarctica) in 2020. This installation had two main seismological goals:

1. to reduce the daytime short periods noise produced from the base and trapped in the firn waveguide ([Albert, 1998](#); [Anthony et al., 2021](#)); and

2. to obtain better horizontal stability of the sensor to avoid regular recentering and improve the noise levels on the horizontal components at long periods.

We also wished to reduce the risks associated with station maintenance and to avoid the snow accumulation that tends to bury buildings in Concordia. The renovation project successfully addressed most of these challenges. First, the new sensor is very stable and does not need the regular recentering required by the instruments in the original vault (see Fig. S1): only one recentering of the T120PH was performed since its installation in January 2020. Second, the overall performance is significantly better than the surface sensors: short-period disturbances and noise levels on the horizontal channels at long periods are both reduced. The CCD borehole station now stands as one of the quietest installations worldwide for periods between 0.2 and 0.6 s and presents some of the lowest noise levels on the horizontal components in Antarctica at periods of around 100 s,

which opens research opportunities for earthquakes studies and normal modes analysis on the horizontal channels. Even at much longer periods, the noise level is quite good on the horizontal components because we are able to record the diurnal and semidiurnal tides (Fig. S5), unlike many stations where the Earth tide signals are hidden by instrument noise and local environmental noise sources (e.g., [Ringler et al., 2020](#)).

We identified atmospheric pressure perturbations that dominate the vertical velocity recordings for periods longer than 1000 s. Based on the values of admittance that we found, the problem likely results from a defect in the atmospheric sealing of the sensor. Because the perturbation is period dependent (see Fig. 7b), the data cannot be corrected by a simple admittance coefficient as typically done for normal modes or gravity studies (e.g., [Crossley et al., 1995](#); [Zürn and Widmer,](#)

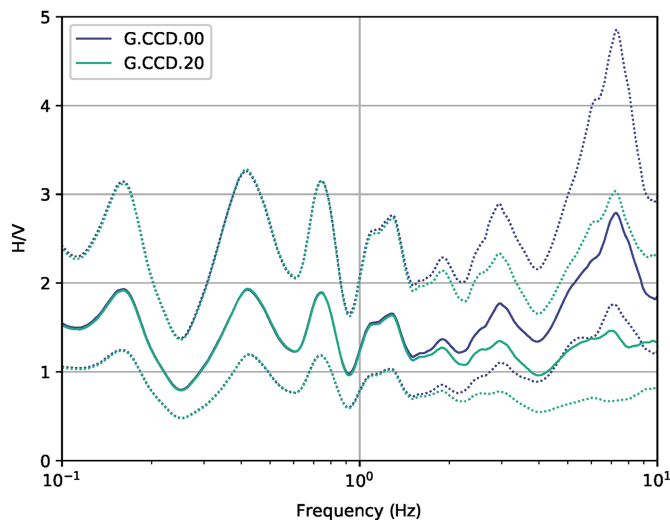


Figure 8. Comparison of horizontal-to-vertical (H/V) spectral ratios (median [solid] and interquartile [dotted] distances) between surface (G.CCD.00) and borehole (G.CCD.20) sensors on 4 hr wide windows fast Fourier transform during whole year 2022. H value is the root mean square of horizontal-components spectra, median and quartile spectra are smoothed over 1/6 decade windows. The color version of this figure is available only in the electronic edition.

1995). To use the vertical components at periods >1000 s would require inverting for the full transfer function (Beauduin *et al.*, 1996), which could be time dependent. Only the vertical component is affected by this problem; very-long-period analyses of the horizontal components are unaffected, as demonstrated in Figure S5. We are evaluating the pertinence of extracting the sensor to test and possibly replace it.

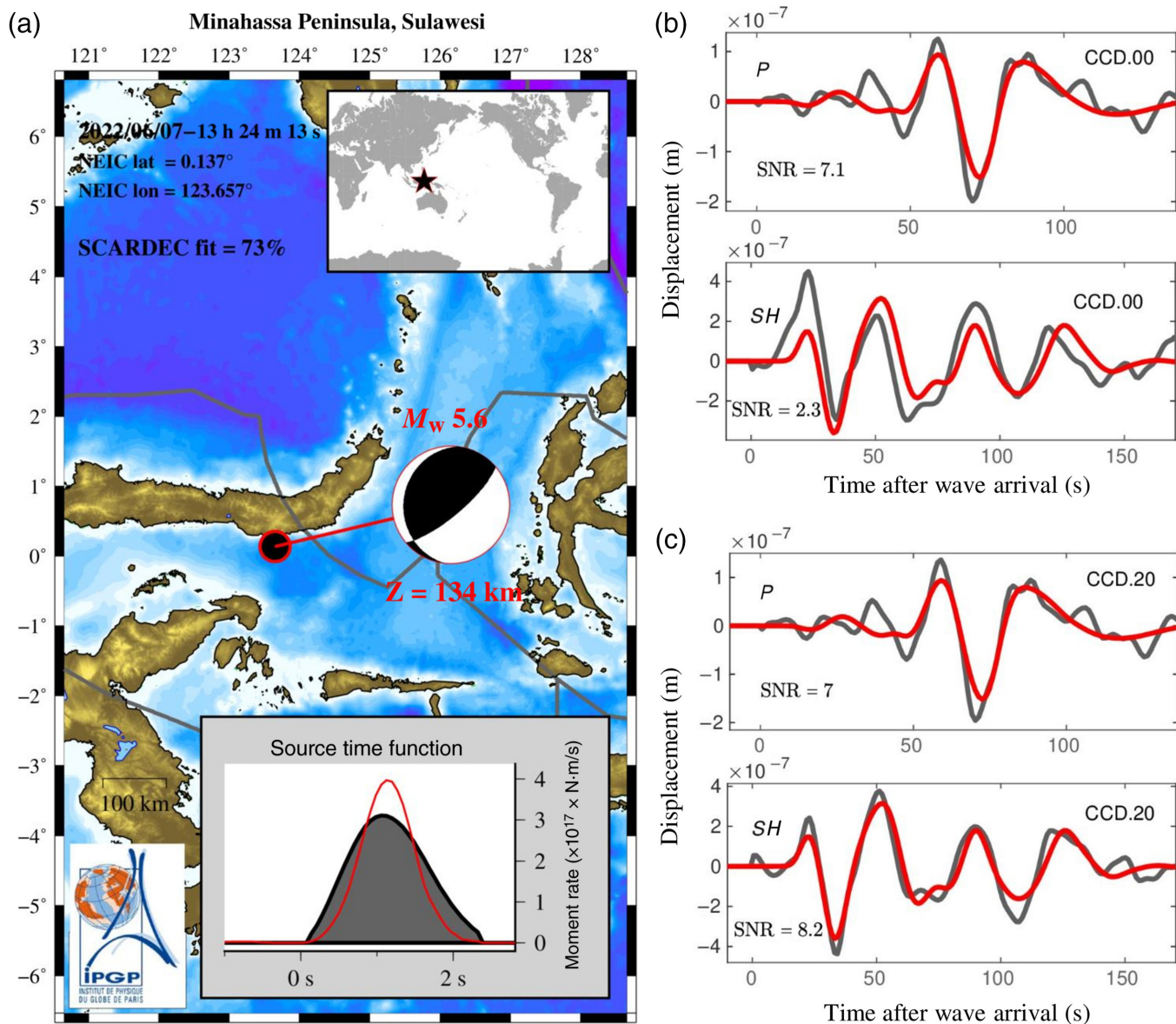
The upgraded CCD borehole station serves as a testament to the collaborative efforts of the scientists, engineers, and organizations involved in the project. The data produced by the CCD borehole station are now distributed as G.CCD.20 by global data centers. We encourage the scientific community to utilize this valuable resource for a wide range of studies requiring seismological recordings from Antarctica, such as tomographic imaging of crustal and mantle structures (e.g., An *et al.*, 2015; Lloyd *et al.*, 2020; Wiens *et al.*, 2023), deep Earth imaging (see Deuss, 2014 and Souriau and Calvet, 2015 for reviews articles), characterization of earthquakes in the southern hemisphere (e.g., Rouland *et al.*, 2003; Reading, 2007; Duputel and Rivera, 2017) or at a global scale (e.g., Ekström *et al.*, 2012; Vallée *et al.*, 2011), analysis of ambient seismic noise sources (e.g., Stutzmann *et al.*, 2009; Grob *et al.*, 2011; Cannata *et al.*, 2019) or analysis of normal modes (see Anthony *et al.*, 2021 for a review of normal-mode analyses from IU.QSPA in Antarctica). These techniques will allow better understanding of the effects of the ice sheet on the topography of East Antarctica, improve estimates of the mantle's viscosity and

its impact on the Earth's crustal response to changes in ice cover mass, and give a more detailed picture of the seismotectonic activity at high latitudes.

Over the past few years, borehole instrumentation for seismological stations has proved efficiency at reducing noise levels, particularly on the horizontal channels (e.g., Hutt *et al.*, 2017; Ringler *et al.*, 2020, 2022). Such infrastructure designs are now used by many network operators at national scales (e.g., the French broadband seismic network or the Hi-Net network in Japan; Réseau Sismologique et géodésique Français [RESIF], 1995; Obara *et al.*, 2005; Vergne *et al.*, 2019) and at global scales. Indeed, GSN has replaced some of its old KS-54000 and STS-1 sensors by STS6-A and T360PH sensors (Albuquerque Seismological Laboratory/USGS, 2014; Ringler *et al.*, 2022) and GEOSCOPE has recently installed a new station in Senegal (SOK) with a STS6-A instrument (see Leroy *et al.*, submitted in the same SRL special edition). In Antarctica, both our new borehole sensor for CCD and the results of IU.QSPA (Anthony *et al.*, 2021) demonstrate the value of investing in boreholes and their related infrastructure to improve noise levels on seismological stations in remote and challenging environments. Future research endeavors can build upon the foundation laid by those successful installations. For example, Anthony *et al.* (2021) explore the feasibility of installing a STS6-A in a pressurized vessel at the ice–bedrock interface in one of the IceCube boreholes. Even if such a setup is not realistically feasible at Concordia, opportunities to instrument deep glaciological boreholes such as EPICA (Augustin *et al.*, 2004) with optical fibers to perform DAS measurements can be explored in the next few years.

Data and Resources

The borehole and the casing installation has been entirely funded and realized by the former Centre de Carottage et Forage National (C2FN), now renamed Plateforme Française de Forage Glaciaire (F2G) available at <https://forage-glaciaire.osug.fr/> of Centre National de la Recherche Scientifique (CNRS). The Institut polaire français Paul-Emile Victor (IPEV) available at <https://institut-polaire.fr/> provided material and personnel logistics, and funded and mounted the shelter on stilts. Seismic instruments were purchased by GEOSCOPE network (Institut de physique du globe de Paris [IPGP] and École et Observatoire des Sciences de la Terre de Strasbourg [EOST], 1982). The seismic data are distributed in real-time (SeedLink protocol at rtserver.ipgp.fr TCP 18000) and via the International Federation of Digital Seismograph Networks (FDSN) webservices by the Institut du Physique du Globe de Paris (IPGP) Data Center available at <https://ws.ipgp.fr/>, at Résif-EPOS (the French contribution to the European Plate Observing System) available at <https://ws.resif.fr/> and at the EarthScope Seismological Facility for the Advancement of Geoscience (SAGE) Facility (Incorporated Research Institutions for Seismology Data Management Center Use [IRIS-DMC]) available at <https://service.iris.edu/>. Catalog of earthquakes and SCARDEC (Vallée *et al.*, 2011) solutions are available at GEOSCOPE website <http://geoscope.ipgp.fr> and twitter available at [@geoscope_ipgp](https://twitter.com/geoscope_ipgp).



Analysis codes used ObsPy (Beyreuther *et al.*, 2010). Trillium 120 posthole seismometer datasheet and manual are available at Nanometrics support webpage <http://support.nanometrics.ca/>. Q330S digitizer datasheet and manual are available at Quanterra website <https://www.q330.com>. STS-2 datasheet and manual are available at Streckeisen website <https://streckeisen.swiss/en/products/sts-2>. All websites were last accessed in August 2023. The supplemental material provides additional figures about the behavior of the posthole sensor, especially at long periods and more detailed pictures about the drilling process.

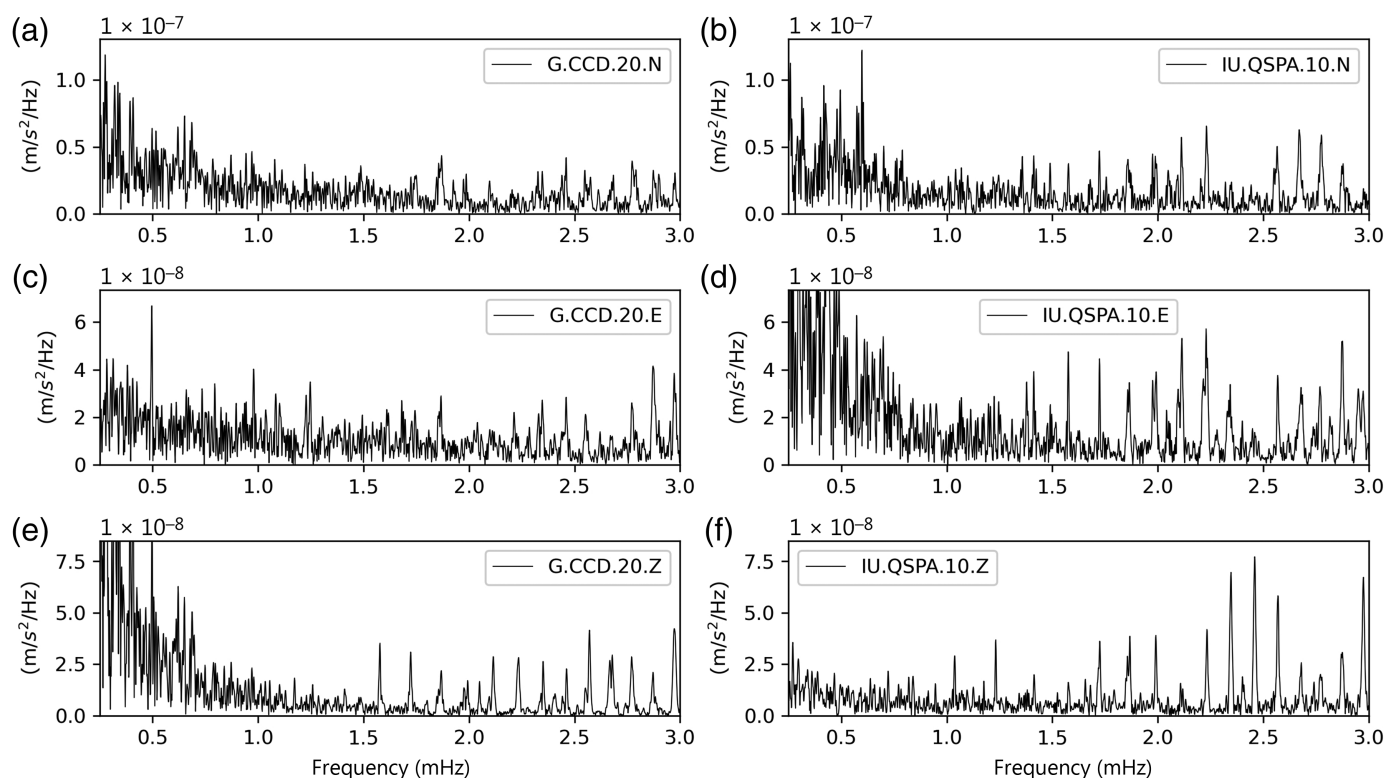
Declaration of Competing Interests

The authors acknowledge that there are no conflicts of interest recorded.

Acknowledgments

The authors thank the French and Italian Polar Institutes for the financial and technical support of this project. The authors want to

Figure 9. (a) Source parameters of the 7 June 2022 M_w 5.6 Sulawesi earthquake determined in near-real time using the SCARDEC method. The top inset displays the earthquake epicentral location on the world map. In the bottom inset, the source time function is shown, both when considering an individual P -wave recording (grey-filled) and when averaging over several P -wave recordings (red curve). (b) Top figure indicates P -wave displacement observed (black) and modeled (red) at the G.CCD.00 surface sensor (vertical component). Both waveforms are filtered in the [0.012–0.04 Hz] frequency range and the signal-to-noise ratio (SNR) based on pre-event signal is shown. Bottom figure indicates same for the SH wave, using the adequate rotation of the G.CCD.00 horizontal components. (c) Same as panel (b) for the G.CCD.20 borehole sensor. Comparison between panels (b) and (c) shows the similar quality of the vertical components and the better quality of the G.CCD.20 horizontal components, both shown by the higher SNR and the better adjustment to synthetics. The color version of this figure is available only in the electronic edition.



acknowledge the huge work performed by all logistical and technical teams in Concordia. Special thanks to Claire Le Calvez, Doris Thuillier, Olivier Haye, Remi Foletto, Armand Patoir, Remi Puaud, Vitto Stanzione, Rocco Acsione, Eric Lefebvre, Gregory Teste, Moreno Baricevic, Marco Buttu, Massimiliano Catricala, Davide Carlucci, Clément Savornin, Christophe Raffin, and the B3D wood construction team. The authors also acknowledge insightful discussion about buoyancy effects with Thomas Forbriger (KIT, BFO). The CCD station would not exist without the great work performed in the late 90s and early 2000s by the team of scientists and engineers at EOST and INGV and more particularly J. Burdin†, D. Rouland†, J. Trampert, and A. Delladio. The CCD seismological observatory station is supported by the following partners: French Polar Institute (IPEV) as part of Project Number 133 Sismologie/OBS, Italian Polar Institute (PNRA), Centre National de la Recherche Scientifique (CNRS) through the Institut des Sciences de l'Univers (INSU), Istituto Nazionale di Geofisica e Vulcanologia (INGV), Ecole et Observatoire des Sciences de la Terre (EOST) from University of Strasbourg, and Institut de Physique du Globe de Paris (IPGP). The authors also thank all the personnel who are supervising the CCD station during the winter. The article benefited from constructive comments by Kyle Smith, an anonymous reviewer, and Editor Adam Ringler.

References

Albert, D. G. (1998). Theoretical modeling of seismic noise propagation in firn at the South Pole, Antarctica, *Geophys. Res. Lett.* **25**, no. 23, 4257–4260, doi: [10.1029/1998GL900155](https://doi.org/10.1029/1998GL900155).

Albuquerque Seismological Laboratory/U.S. Geological Survey (USGS) (2014). Global seismograph network, GSN—IRIS/USGS, doi: [10.7914/SN/IU](https://doi.org/10.7914/SN/IU).

Figure 10. Example of Fourier spectra for the Earth free oscillations in the frequency band 0.25–3 mHz (periods between 330 and 4000s) for the 29 June 2021 Alaska peninsula earthquake (M_w 8.2) recorded by (a,c,e) the borehole seismometer, and (b,d,f) the CGM3-T of QSPA. Data were processed using a three-day time window, starting one hour after the origin time. A hanning window and a zero padding of 3 times the length of the data time window were applied prior processing. Horizontal components were rotated for comparison as both sensors have not the same orientation.

An, M., D. A. Wiens, Y. Zhao, M. Feng, A. A. Nyblade, M. Kanao, Y. Li, A. Maggi, and J.-J. Lévêque (2015). S-velocity model and inferred Moho topography beneath the Antarctic plate from Rayleigh waves, *J. Geophys. Res.* **120**, no. 1, 359–383, doi: [10.1002/2014jb011332](https://doi.org/10.1002/2014jb011332).

Anderson, K. (2003). *Seismic Noise Trapping in Firn, Theoretical Seismology Class Presentation*, New Mexico Tech, Department of Earth and Environmental Science, Socorro, New Mexico.

Anthony, R. E., A. T. Ringler, M. DuVernois, K. R. Anderson, and D. C. Wilson (2021). Six decades of seismology at South Pole, Antarctica: Current limitations and future opportunities to facilitate new geophysical observations, *Seismol. Res. Lett.* **92**, no. 5, 2718–2735, doi: [10.1785/0220200448](https://doi.org/10.1785/0220200448).

Augustin, L., C. Barbante, P. R. F. Barnes, J. Marc Barnola, M. Bigler, E. Castellano, O. Cattani, J. Chappellaz, D. Dahl-Jensen, *et al.* (2004). Eight glacial cycles from an Antarctic ice core, *Nature* **429**, no. 6992, 623–628, doi: [10.1038/nature02599](https://doi.org/10.1038/nature02599).

Bard, P.-Y. (1998). Microtremor measurements: A tool for site effect estimation? *The Effects of Surface Geology on Seismic Motion*, Yokohama, Japan, December 1998, Vol. 3, 1251–1279.

- Beauduin, R., P. Lognonné, J. P. Montagner, S. Cacho, J. F. Karczewski, and M. Morand (1996). The effects of the atmospheric pressure changes on seismic signals or how to improve the quality of a station, *Bull. Seismol. Soc. Am.* **86**, no. 6, 1760–1769, doi: [10.1785/BSSA0860061760](https://doi.org/10.1785/BSSA0860061760).
- Benz, H. (2017). Building a National Seismic Monitoring Center: NEIC from 2000 to the present, *Seismol. Res. Lett.* **88**, no. 2B, 457–461, doi: [10.1785/0220170034](https://doi.org/10.1785/0220170034).
- Beyreuther, M., R. Barsch, L. Krischer, T. Megies, Y. Behr, and J. Wassermann (2010). ObsPy: A python toolbox for seismology, *Seismol. Res. Lett.* **81**, no. 3, 530–533, doi: [10.1785/gssrl.81.3.530](https://doi.org/10.1785/gssrl.81.3.530).
- Bréant, C., P. Martinerie, A. Orsi, L. Arnaud, and A. Landais (2017). Modelling firn thickness evolution during the last deglaciation: Constraints on sensitivity to temperature and impurities, *Clim. Past* **13**, no. 7, 833–853, doi: [10.5194/cp-13-833-2017](https://doi.org/10.5194/cp-13-833-2017).
- Cannata, A., F. Cannavò, S. Moschella, S. Gresta, and L. Spina (2019). Exploring the link between microseism and sea ice in Antarctica by using machine learning, *Sci. Rep.* **9**, no. 1, 1–15, doi: [10.1038/s41598-019-49586-z](https://doi.org/10.1038/s41598-019-49586-z).
- Crossley, D., O. Jensen, and J. Hinderer (1995). Effective barometric admittance and gravity residuals, *Phys. Earth Planet. In.* **90**, 221–241, doi: [10.1016/0031-9201\(95\)05086-Q](https://doi.org/10.1016/0031-9201(95)05086-Q).
- Deuss, A. (2014). Heterogeneity and anisotropy of earth's inner core, *Annu. Rev. Earth Planet. Sci.* **42**, no. 1, 103–126, doi: [10.1146/annurev-earth-060313-054658](https://doi.org/10.1146/annurev-earth-060313-054658).
- Diez, A., O. Eisen, C. Hofstede, P. Bohléber, and U. Polom (2013). Joint interpretation of explosive and vibroseismic surveys on cold firn for the investigation of ice properties, *Ann. Glaciol.* **54**, no. 64, 201–210, doi: [10.3189/2013AoG64A200](https://doi.org/10.3189/2013AoG64A200).
- Duputel, Z., and L. Rivera (2017). Long-period analysis of the 2016 Kaikoura earthquake, *Phys. Earth Planet. In.* **265**, 62–66, doi: [10.1016/j.pepi.2017.02.004](https://doi.org/10.1016/j.pepi.2017.02.004).
- Ekström, G., M. Nettles, and A. M. Dziewoński (2012). The global CMT project 2004–2010: Centroid-moment tensors for 13,017 earthquakes, *Phys. Earth Planet. In.* **200–201**, 1–9, doi: [10.1016/j.pepi.2012.04.002](https://doi.org/10.1016/j.pepi.2012.04.002).
- Ewing, M., and F. Press (1953). Further study of atmospheric pressure fluctuations recorded on seismographs, *Eos Trans. AGU* **34**, no. 1, 95–100, doi: [10.1029/TR034i001p00095](https://doi.org/10.1029/TR034i001p00095).
- Field, E. H., and K. H. Jacob (1995). A comparison and test of various site-response estimation techniques, including three that are not reference-site dependent, *Bull. Seismol. Soc. Am.* **85**, no. 4, 1127–1143.
- Gitterman, Y., Y. Zaslavsky, A. Shapira, and V. Shtivelman (1996). Empirical site response evaluations: Case studies in Israel, *Soil Dynam. Earthq. Eng.* **15**, no. 7, 447–463, doi: [10.1016/0267-7261\(96\)00019-X](https://doi.org/10.1016/0267-7261(96)00019-X).
- Grob, M., A. Maggi, and E. Stutzmann (2011). Observations of the seasonality of the Antarctic microseismic signal, and its association to sea ice variability, *Geophys. Res. Lett.* **38**, no. 11, doi: [10.1029/2011GL047525](https://doi.org/10.1029/2011GL047525).
- Helmholtz-Centre Potsdam—GeoForschungsZentrums (GFZ) German Research Centre for Geosciences and gempa GmbH (2008). The SeisComP seismological software package, GFZ Data Services, doi: [10.5880/GFZ.2.4.2020.003](https://doi.org/10.5880/GFZ.2.4.2020.003).
- Hutt, C. R., A. T. Ringler, and L. S. Gee (2017). Broadband seismic noise attenuation versus depth at the Albuquerque seismological laboratory, *Bull. Seismol. Soc. Am.* **107**, no. 3, 1402–1412, doi: [10.1785/0120160187](https://doi.org/10.1785/0120160187).
- Institut de physique du globe de Paris (IPGP) and École et Observatoire des Sciences de la Terre de Strasbourg (EOST) (1982). GEOSCOPE, French global network of broadband seismic stations, doi: [10.18715/GEOSCOPE.G](https://doi.org/10.18715/GEOSCOPE.G).
- Lermo, J., and F. J. Chávez-García (1993). Site effect evaluation using spectral ratios with only one station, *Bull. Seismol. Soc. Am.* **83**, no. 5, 1574–1594.
- Lévêque, J.-J., A. Maggi, and A. Souriau (2010). Seismological constraints on ice properties at dome C, Antarctica, from horizontal to vertical spectral ratios, *Antarct. Sci.* **22**, no. 5, 572–579, doi: [10.1017/S0954102010000325](https://doi.org/10.1017/S0954102010000325).
- Lloyd, A. J., D. A. Wiens, H. Zhu, J. Tromp, A. A. Nyblade, A. A. Nyblade, R. C. Aster, S. E. Hansen, I. W. D. Dalziel, T. J. Wilson, et al. (2020). Seismic structure of the Antarctic Upper Mantle imaged with adjoint tomography, *J. Geophys. Res.* **125**, no. 3, doi: [10.1029/2019JB017823](https://doi.org/10.1029/2019JB017823).
- McNamara, D. E. (2004). Ambient noise levels in the continental United States, *Bull. Seismol. Soc. Am.* **94**, no. 4, 1517–1527, doi: [10.1785/012003001](https://doi.org/10.1785/012003001).
- Moulik, P., and G. Ekström (2014). An anisotropic shear velocity model of the earth's mantle using normal modes, body waves, surface waves and long-period waveforms, *Geophys. J. Int.* **199**, no. 3, 1713–1738, doi: [10.1093/gji/ggu356](https://doi.org/10.1093/gji/ggu356).
- Nakamura, Y. (1989). A method for dynamic characteristics estimation of subsurface using microtremor on the ground surface, *Q. Rep. Railway Tech. Res. Inst.* **30**, 25–33.
- Obara, K., K. Kasahara, S. Hori, and Y. Okada (2005). A densely distributed high-sensitivity seismograph network in Japan: Hi-net by national research institute for earth science and disaster prevention, *Rev. Sci. Instrum.* **76**, no. 2, 021301, doi: [10.1063/1.1854197](https://doi.org/10.1063/1.1854197).
- Peterson, J. R. (1993). Observations and modeling of seismic background noise, *U.S. Geol. Surv. Rept.* 93322, doi: [10.3133/ofr93322](https://doi.org/10.3133/ofr93322).
- Reading, A. M. (2007). The seismicity of the Antarctic plate, in *Continental Intraplate Earthquakes: Science, Hazard, and Policy Issues*, Geological Society of America, doi: [10.1130/2007.2425\(18\)](https://doi.org/10.1130/2007.2425(18)).
- Réseau Sismologique et géodésique Français (RESIF) (1995). RESIF-RLBP French broad-band network, RESIF-RAP strong motion network and other seismic stations in metropolitan France [Data set], doi: [10.15778/RESIF.FR](https://doi.org/10.15778/RESIF.FR).
- Restelli, F., P. Koelemeijer, and A. M. G. Ferreira (2023). Normal mode observability of radial anisotropy in the earth's Mantle, *Geophys. J. Int.* **233**, no. 1, 663–679, doi: [10.1093/gji/ggac474](https://doi.org/10.1093/gji/ggac474).
- Ringler, A. T., R. E. Anthony, R. C. Aster, C. J. Ammon, S. Arrowsmith, H. Benz, C. Ebeling, A. Frassetto, W.-Y. Kim, P. Koelemeijer, et al. (2022). Achievements and prospects of global broadband seismographic networks after 30 years of continuous geophysical observations, *Rev. Geophys.* **60**, no. 3, e2021RG000749, doi: [10.1029/2021RG000749](https://doi.org/10.1029/2021RG000749).
- Ringler, A. T., J. Steim, D. C. Wilson, R. Widmer-Schmidrig, and R. E. Anthony (2020). Improvements in seismic resolution and current limitations in the global seismographic network, *Geophys. J. Int.* **220**, no. 1, 508–521, doi: [10.1093/gji/ggz473](https://doi.org/10.1093/gji/ggz473).
- Romanowicz, B., and H.-R. Wenk (2017). Anisotropy in the deep earth, *Phys. Earth Planet. In.* **269**, 58–90, doi: [10.1016/j.pepi.2017.05.005](https://doi.org/10.1016/j.pepi.2017.05.005).

- Rouland, D., C. Condis, and G. Roullet (2003). Overlooked earthquakes on and around the Antarctica plate: Identification and location of 1999 shallow depth events, *Tectonophysics* **376**, no. 1, 117, doi: [10.1016/j.tecto.2003.08.006](https://doi.org/10.1016/j.tecto.2003.08.006).
- Schneider, S., and A. Deuss (2021). A new catalogue of toroidal-mode overtone splitting function measurements, *Geophys. J. Int.* **225**, no. 1, 329–341, doi: [10.1093/gji/ggaa567](https://doi.org/10.1093/gji/ggaa567).
- Seekins, L. C., L. Wennerberg, L. Margheriti, and H.-P. Liu (1996). Site amplification at five locations in San Francisco, California: A comparison of S waves, codas, and microtremors, *Bull. Seismol. Soc. Am.* **86**, no. 3, 627–635.
- Souriau, A., and M. Calvet (2015). 1.23—Deep earth structure: The earth's cores, in *Treatise on Geophysics*, G. Schubert (Editor), Second Ed., Elsevier, 725–757, doi: [10.1016/B978-0-444-53802-4.00020-8](https://doi.org/10.1016/B978-0-444-53802-4.00020-8).
- Souriau, A., A. Roullé, and C. Ponsolles (2007). Site effects in the City of Lourdes, France, from H/V measurements: Implications for seismic-risk evaluation, *Bull. Seismol. Soc. Am.* **97**, no. 6, 2118–2136, doi: [10.1785/0120060224](https://doi.org/10.1785/0120060224).
- Stutzmann, E., M. Schimmel, G. Patau, and A. Maggi (2009). Global climate imprint on seismic noise, *Geochem. Geophys. Geosys.* **10**, no. 11, doi: [10.1029/2009GC002619](https://doi.org/10.1029/2009GC002619).
- Tromp, J., and E. Zankerka (1995). Toroidal splitting observations from the great 1994 Bolivia and Kuril Islands earthquakes, *Geophys. Res. Lett.* **22**, 2297–2300, doi: [10.1029/95GL01810](https://doi.org/10.1029/95GL01810).
- Vallée, M., J. Charléty, A. M. G. Ferreira, B. Delouis, and J. Vergoz (2011). SCARDEC: A new technique for the rapid determination of seismic moment magnitude, focal mechanism and source time functions for large earthquakes using body-wave deconvolution, *Geophys. J. Int.* **184**, no. 1, 338–358.
- Vergne, J., H. Pauchet, M. Bonnin, E.-M. Aissaoui, L. Ardito, J. Battaglia, S. Baudin, S. Benahmed, M. B. de Berc, E. Beucler, *et al.* (2019). Quality improvement of the French permanent broadband stations with shallow posthole installations, *EGU General Assembly 2019*, Vienna, Austria, April 2019.
- Wielandt, E., and G. Streckeisen (1982). The leaf-spring seismometer: Design and performance, *Bull. Seismol. Soc. Am.* **72**, 2349–2367.
- Wiens, D. A., W. Shen, and A. J. Lloyd (2023). *The Seismic Structure of the Antarctic Upper Mantle*, Geological Society, London, Memoirs, 195–212, doi: [10.1144/M56-2020-18](https://doi.org/10.1144/M56-2020-18).
- Zürn, W., and R. Widmer (1995). On noise reduction in vertical seismic records below 2 mHz using barometric pressure, *Geophys. Res. Lett.* **22**, no. 24, 3537–3540, doi: [10.1029/95GL03369](https://doi.org/10.1029/95GL03369).
- Zürn, W., and E. Wielandt (2007). On the minimum of vertical seismic noise near 3 mHz, *Geophys. J. Int.* **168**, 647–658, doi: [10.1111/j.1365-246x.2006.03189.x](https://doi.org/10.1111/j.1365-246x.2006.03189.x).
- Zürn, W., T. Forbriger, R. Widmer-Schnidrig, P. Duffner, and A. T. Ringler (2022). Modelling tilt noise caused by atmospheric processes at long periods for several horizontal seismometers at BFO—A reprise, *Geophys. J. Int.* **228**, no. 2, 927–943, doi: [10.1093/gji/ggab336](https://doi.org/10.1093/gji/ggab336).

Manuscript received 14 June 2023
Published online 29 September 2023